Journal of Magnetic Resonance 200 (2009) 198–206

Contents lists available at ScienceDirect

Journal of Magnetic Resonance

journal homepage: www.elsevier.com/locate/jmr

A rapid measurement of T_1/T_2: The DECPMG sequence

J. Mitchell [a], M.D. Hürlimann [b], E.J. Fordham [c,*]

[a] Department of Chemical Engineering and Biotechnology, University of Cambridge, Pembroke Street, Cambridge CB2 3RA, United Kingdom
[b] Schlumberger-Doll Research Center, 1 Hampshire Street, Cambridge, MA 02139-1578, USA
[c] Schlumberger Cambridge Research, High Cross, Madingley Road, Cambridge CB3 0HG, United Kingdom

ARTICLE INFO

Article history:
Received 25 March 2009
Revised 25 June 2009
Available online 7 July 2009

Keywords:
Driven equilibrium
T_1/T_2
Relaxation correlations
Surface residency times
Laplace transforms
Reservoir rocks

ABSTRACT

The Driven-Equilibrium Carr–Purcell Meiboom–Gill (DECPMG) pulse sequence is a rapid method for obtaining the average ratio of longitudinal to transverse relaxation times $\langle T_1/T_2 \rangle$ as a function of T_2. Since this is a one-dimensional experiment, the $\langle T_1/T_2 \rangle_{T_2}$ ratio can be acquired, potentially, in just two scans; the second scan being a reference CPMG measurement. Conventionally, T_1/T_2 is determined from a two-dimensional $T_1 - T_2$ relaxation correlation experiment. The method described here offers a significant reduction in experimental time without a reduction in signal-to-noise. The $\langle T_1/T_2 \rangle$ ratio is useful for comparing the behaviour of liquids in porous media. Here we demonstrate the application of the DECPMG sequence to the study of oil-bearing rocks by differentiating oil or water saturated rock cores, and by observing the relative strengths of surface interaction for water in two types of rock by measuring $\langle T_1/T_2 \rangle$ as a function of magnetic field strength.

1. Introduction

Two-dimensional Nuclear Magnetic Resonance (NMR) relaxation or diffusion correlations have become a popular tool for characterising porous media. This is possible due to the implementation of a fast computational algorithm to solve Fredholm integrals (so-called "inverse Laplace transforms") numerically in two-dimensions by Venkataramanan et al. [1]. The correlation or exchange experiments now include $T_1 - T_2$ [2], $T_2 - T_1 - \delta$ [3], $D - T_2$ [4], $T_2 - T_2$ [5,6], $T_1 - T_1 - \delta$ [3], and $D - D$ [7], where T_1 and T_2 refer to the longitudinal and transverse spin relaxation times, respectively, δ is chemical shift, and D is the self-diffusion coefficient. These experiments have been used extensively in the study of oil-bearing rocks [8]. The $D - T_2$ correlation is particularly useful when implemented on low-field or portable magnet systems, such as NMR well-logging tools [9,10], since it allows oil and water components to be distinguished without chemical shift information. $T_1 - T_2$ correlations can also be used to identify oil and water fractions if the aqueous and organic components have different relaxation times. The conventional $T_1 - T_2$ correlation experiments can be time consuming, particularly if the signal-to-noise ratio (S/N) is poor, as is common on low-field systems, therefore requiring extensive signal averaging. In some experiments only the ratio T_1/T_2 is required and this can be determined without acquiring a two-dimensional data set. For example, when measured as a function of magnetic field strength, T_1/T_2 can be used to estimate the residency times of molecules on a pore surface [11]. T_1/T_2 can also be used to infer relative strengths of surface interaction for different liquids in pores [12], and can be used to remove relaxation time weighting in NMR flow propagator measurements [13].

In this paper we describe a rapid method of determining the average ratio of relaxation times $\langle T_1/T_2 \rangle$ as a function of T_2. The Driven-Equilibrium Carr–Purcell Meiboom–Gill (DECPMG) pulse sequence [14] provides a CPMG echo train with the initial signal amplitude reduced to an equilibrium magnetisation M_{de}. The $\langle T_1/T_2 \rangle$ ratio is related to the ratio of the equilibrium to total magnetisation M_{de}/M_0, where M_0 is obtained from a standard CPMG [15,16] reference scan. The $\langle T_1/T_2 \rangle$ ratio can be determined as a function of T_2 using a conventional one-dimensional numerical inversion to generate a distribution of T_2 relaxation time components from the echo trains.

Whilst other techniques have been proposed for determining T_1/T_2, these have limitations, including the accurate calibration of small tip angle radio frequency (rf) pulses [17] or chemical shift interactions [18], or only measure long T_1 components [19], or require complicated data analysis [20]. The DECPMG pulse sequence does not suffer from any of these limitations. In addition, this method can be applied directly to systems that consist of many components with different relaxation times. As long as the components have distinguishable T_2 relaxation times, the individual T_1/T_2 ratio can be extracted for all components simultaneously, without the need for additional data acquisitions.

* Corresponding author.
E-mail address: fordham@cambridge.oilfield.slb.com (E.J. Fordham).

1090-7807/$ - see front matter © 2009 Elsevier Inc. All rights reserved.
doi:10.1016/j.jmr.2009.07.002

The DECPMG sequence is based on the Driven Equilibrium Fourier Transform (DEFT) pulse sequence [21], proposed as a sensitivity enhancement in NMR spectroscopy. DEFT allows the repeat acquisition of a spectrum without having to wait for the spins to recover on the longitudinal axis. This is achieved by applying a 180° rf pulse after the acquisition of a free induction decay (FID — the signal following an excitation pulse of, typically, 90°). This causes a spin echo to form [22], wherein the dephased spin ensemble is refocused. A second 90° pulse is applied of opposite phase to the excitation pulse at the centre of the echo to rotate the coherent spin ensemble back onto the $+z$-axis ready for the next acquisition. This is suitable for samples where both T_1 and T_2 are approximately equal. In systems where $T_2 \ll T_1$ the sensitivity enhancement is less significant due to transverse relaxation over the acquisition interval [23]. For this reason, other sensitivity enhancement techniques have proven more popular in spectroscopic applications [24]. In contrast, the DECPMG pulse sequence functions for a wide range of T_1 and T_2 times. The experimental timings can be optimised to provide a good signal-to-noise ratio (S/N) since the equilibrium magnetisation M_{de} depends on the relative duration of the relaxation intervals in the pulse sequence. We discuss the frequency dependence of M_{de} and the applicability of the technique to inhomogeneous magnetic fields. Examples are presented that highlight potential uses of the DECPMG sequence in the study of oil reservoir rocks.

2. The DECPMG pulse sequence

In a standard Carr–Purcell–Meiboom–Gill (CPMG) measurement, the application of the rf pulses is preceded by a recycle delay T_w that is assumed to be long compared to the longest T_1 relaxation time component ($T_{1,\mathrm{long}}$) in the sample. Ideally, $T_w \geqslant 5 \times T_{1,\mathrm{long}}$. This ensures that the magnetisation has reached thermal equilibrium before the CPMG pulse sequence is applied. In our approach, we compare this standard CPMG measurement with the DECPMG pulse sequence shown in Fig. 1 that consists of two parts: an initial Driven-Equilibrium (DE) portion, followed by a CPMG echo train. In the DECPMG sequence, T_w associated with the standard CPMG sequence is replaced by a long series of rf pulses that places the spin ensemble in a driven equilibrium that is different to the thermal equilibrium. The total duration of the DE portion should be comparable to T_w to ensure the driven equilibrium is obtained.

2.1. Driven equilibrium

The DE portion consists of repeated [excite-echo-store] units that transfer the magnetisation from the longitudinal direction to the transverse plane for a duration τ_2 and then restore it to the longitudinal direction for a duration τ_1. In the implementation shown in Fig. 1, this is achieved by an initial 90° pulse followed by two 180° refocusing pulses and a second 90° pulse centred on the second echo. This cycle is repeated p times in each scan until the magnetisation reaches a dynamic or driven equilibrium M_{de}. Ideally, the durations τ_1 and τ_2 are much shorter than the longitudinal and transverse relaxation times T_1 and T_2. This condition is referred to as the fast pulsing regime. Fast pulsing simplifies the analysis of the experiment greatly, and has the added benefit of minimising complications due to diffusion or J-coupling [25].

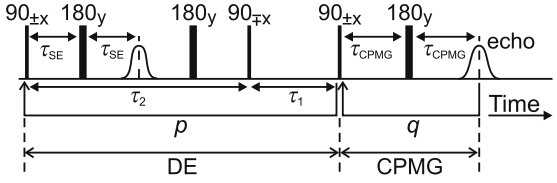

Fig. 1. The DECPMG pulse sequence. The DE portion of the sequence is repeated p times whilst the CPMG portion is repeated q times. The driven equilibrium is obtained after p repetitions of the DE portion of the pulse sequence.

The approach to the driven equilibrium magnetisation M_{de} can be monitored by detecting the amplitudes of the echoes that form in the middle of every τ_2 period. For ideal on-resonance pulses, the echo amplitude M_P after P cycles approaches the equilibrium magnetisation as follows:

$$M_P = M_{de} + (M_{P=0} - M_{de}) \exp\left\{-P\left(\frac{\tau_1}{T_1} + \frac{\tau_2}{T_2}\right)\right\}, \tag{1}$$

where $M_{P=0}$ is the initial longitudinal magnetisation. In the fast pulsing regime, the equilibrium magnetisation M_{de} is given by:

$$M_{de} = M_0 \frac{1}{1 + \frac{T_1}{T_2}\frac{\tau_2}{\tau_1}}. \tag{2}$$

Note that the equilibrium magnetisation only depends on the ratio of the relaxation times T_1/T_2, not on the absolute values of the relaxation times. The driven equilibrium is obtained once the T_2 decay of the transverse magnetisation across $\tau_2(\Delta M_\perp)$ is compensated exactly by the T_1 build-up of the longitudinal magnetisation across $\tau_1(\Delta M_z)$. In the fast pulsing regime, the linear approximations $\Delta M_\perp = -\frac{\tau_2}{T_2} M_p$ and $\Delta M_z = +\frac{\tau_1}{T_1}(M_0 - M_p)$ can be used. Requiring $\Delta M_\perp = -\Delta M_z$ in the driven equilibrium implies that M_p is given by the equilibrium magnetisation M_{de} in Eq. (2).

Outside of the fast pulsing regime, when the durations τ_1 and τ_2 approach or exceed the relaxation times, the linear approximations become inaccurate and the general expression for the equilibrium magnetisation is then given by:

$$M_{de} = M_0 \frac{1 - \Gamma_{1,1}}{1 - \Gamma_{1,1}\Gamma_{2,2}}, \tag{3}$$

where $\Gamma_{i,j} \equiv \exp\{-\tau_i/T_j\}$. In the fast pulsing regime ($\tau_1 \ll T_1$; $\tau_2 \ll T_2$), this expression reduces to Eq. (2).

2.2. CPMG detection

The DECPMG sequence is formed by appending a CPMG echo train to the initial DE preconditioning segment. It is assumed that the number of cycles in the DE segment exceeds $P \gg (\tau_1/T_1 + \tau_2/T_2)^{-1}$ so that the equilibrium magnetisation is obtained. This can be verified by monitoring the time dependence of the echo amplitudes during the DE segment. In addition, it is assumed that the fast pulsing regime applies. The amplitudes of the qth echo in the CPMG train of the DECPMG sequence is then given by

$$M_D(qt_E) = M_{de} \exp\left\{-\frac{qt_E}{T_2}\right\} = M_0 \frac{1}{1 + \frac{T_1}{T_2}\frac{\tau_2}{\tau_1}} \exp\left\{-\frac{qt_E}{T_2}\right\}. \tag{4}$$

Here $t_E = 2\tau_{CPMG}$ is the spin echo spacing in the CPMG train. By comparing these amplitudes generated by the DECPMG sequence with those generated by the standard CPMG sequence where

$$M_C(qt_E) = M_0 \exp\left\{-\frac{qt_E}{T_2}\right\}, \tag{5}$$

the ratio of the transverse and longitudinal relaxation times T_1/T_2 can be determined from

$$\frac{T_1}{T_2} = \frac{\tau_1}{\tau_2}\left(\frac{M_C}{M_D} - 1\right). \tag{6}$$

In addition to this ratio, the relaxation time T_2 can be extracted from the decay of the echo amplitudes $M_D(qt_E)$ or $M_C(qt_E)$. The combination of these quantities therefore allows the determination of the longitudinal relaxation time T_1 from only two measurements.

In principle, it is possible to obtain this information from the analysis of the driven equilibrium sequence alone, as was pointed out previously by Edzes [26]. However, this approach assumes implicitly that the relaxation behaviour of the sample can be described accurately by single relaxation time components in T_1 and T_2. The full benefit of the DECPMG sequence becomes evident when we consider multi-component or heterogeneous systems that cannot be characterised by single T_1 and T_2 relaxation times.

2.3. Multiple discrete relaxation time components

Many systems of interest are complex or heterogeneous and the relaxation behaviour often deviates significantly from a single-exponential decay. In a system containing multiple components i with corresponding relative amplitudes A_i and relaxation times $T_{2,i}$, the magnetisation decay becomes $M(t) = \sum A_i \exp\{-t/T_{2,i}\}$.

In this way, the DECPMG method is applicable to heterogeneous samples. It requires first a decomposition of the echo decay into the individual $T_{2,i}$ relaxation time components. This allows the determination of the T_1/T_2 ratio for each $T_{2,i}$ component by comparing the separate measured DECPMG amplitude $A_{D,i}$ with that of the standard CPMG sequence $A_{C,i}$. The DECPMG method is sensitive to a wide range of relaxation times and allows the extraction of T_1 and T_2 information with only two measurements. In contrast, standard inversion or saturation-recovery techniques [27] require multiple measurements with different recovery times that explore the whole range of relaxation times.

2.4. Distribution of relaxation times

In many samples, it is not possible to decompose the signal unambiguously into discrete components and it is more appropriate to use continuous distributions to describe the system. Since the relaxation times can span several orders of magnitude, it is convenient to use a logarithmic scale for the relaxation times and fit the measured echo amplitudes of the DECPMG (D) or CPMG (C) sequence to:

$$M_{D,C}(t) = \int \mathrm{d}\log T_2 A_{D,C}(\log T_2) \exp\left\{-\frac{t}{T_2}\right\}. \tag{7}$$

The distribution functions $A_{D,C}(\log T_2)$ are extracted from the measured amplitudes using a numerical inverse with a regularisation parameter that controls the trade-off between instability and bias [28]. It is sensible to use the same regularisation parameter κ for both data sets. The optimum value of κ should be selected from the DECPMG data as this has the lower S/N and it can be selected using the Butler–Reeds–Dawson (BRD) [29], or Generalised Cross Validation (GCV) [30,31] methods.

Formally, the distribution of T_1 and T_2 relaxation times in a sample can be characterised by the two-dimensional distribution function $f_2(\log T_2, T_1/T_2)$. The response of the DECPMG sequence is then given by:

$$M_D(qt_E) = \int\int \mathrm{d}\log T_2 \,\mathrm{d}\frac{T_1}{T_2} \frac{1}{1+\frac{\tau_2}{\tau_1}\frac{T_1}{T_2}} f_2\left(\log T_2, \frac{T_1}{T_2}\right) \exp\left\{-\frac{qt_E}{T_2}\right\}. \tag{8}$$

The distribution function $f_2(\log T_2, T_1/T_2)$ is related directly to the more frequently used distribution function in terms of $g_2(\log T_2, \log T_1)$ [2] by a simple Jacobian, i.e.

$$f_2\left(\log T_2, \frac{T_1}{T_2}\right) = \frac{T_2}{T_1} g_2(\log T_2, \log T_1). \tag{9}$$

In many cases, the distribution is rather narrow along the T_1/T_2 axis and the expression in Eq. (8) can be reduced to a one-dimensional distribution:

$$M_D(qt_E) \simeq \int\int \mathrm{d}\log T_2 \frac{1}{1+\frac{\tau_2}{\tau_1}\left\langle\frac{T_1}{T_2}\right\rangle_{T_2}} f_1(\log T_2) \exp\left\{-\frac{qt_E}{T_2}\right\}. \tag{10}$$

The ratio of the longitudinal to transverse relaxation times is given here by

$$\langle T_1/T_2\rangle_{T_2} \equiv \frac{1}{f_1(\log T_2)} \int \mathrm{d}\frac{T_1}{T_2} f_2\left(\log T_2, \frac{T_1}{T_2}\right)\frac{T_1}{T_2}, \tag{11}$$

for the components characterised by the transverse relaxation time T_2. In addition, $f_1(\log T_2)$ is the one-dimensional distribution function of the T_2 relaxation time that can also be viewed as the projection of the two-dimensional distribution functions onto the T_2 axis:

$$f_1(\log T_2) = \int f_2\left(\log T_2, \frac{T_1}{T_2}\right)\mathrm{d}\frac{T_1}{T_2} = \int g_2(\log T_2, \log T_1)\mathrm{d}\log T_1. \tag{12}$$

Comparison of Eq. (10) with the expression in Eq. (7) shows that the extracted distribution function for the DECPMG sequence, A_D, corresponds to:

$$A_D(\log T_2) = \frac{1}{1+\frac{\tau_2}{\tau_1}\left\langle\frac{T_1}{T_2}\right\rangle_{T_2}} f_1(\log T_2). \tag{13}$$

The one-dimensional distribution function can be determined independent of the standard CPMG measurement, as the extracted distribution function corresponds directly to $A_C(\log T_2) = f_1(\log T_2)$. Even in heterogeneous systems, it is therefore possible to extract the ratio of relaxation times $\langle T_1/T_2\rangle_{T_2}$ as a function of T_2 from just two measurements by analysis of the ratio of $A_D(\log T_2)$ and $A_C(\log T_2)$:

$$\left\langle\frac{T_1}{T_2}\right\rangle_{T_2} = \frac{\tau_1}{\tau_2}\left[\frac{A_C(\log T_2)}{A_D(\log T_2)} - 1\right]. \tag{14}$$

If, for a given T_2 there is a wide distribution of T_1/T_2 values, the approximation used in the deviation of Eqs. (10)–(14) tends to underestimate the true average value $\langle T_1/T_2\rangle_{T_2}$. In such cases, based on Eq. (8), it is in principle possible to extract the full two-dimensional distribution function $f_2(\log T_2, T_1/T_2)$ from multiple DECPMG measurements with different ratios of τ_1/τ_2, and hence determine $g_2(\log T_2, \log T_1)$. This requires a two-dimensional inversion of $M_D(\tau_1/\tau_2, qt_E)$. However, in this case, the total acquisition time will approach that of a standard inversion-recovery $T_1 - T_2$ correlation experiment and the intrinsic advantage disappears. In addition, the extraction of full T_1 distribution functions from DECPMG experiments is less robust, typically, than from inversion-recovery experiments with comparable S/N ratios. The main reason is that the kernel for the DECPMG experiments is exponential only with respect to T_2, but algebraic with respect to T_1/T_2. In contrast, the kernels for the $T_1 - T_2$ experiment are exponential in both dimensions.

Recently, a "double-shot" method of acquiring accurate, quantitative distributions of T_1 relaxation times in just two scans was demonstrated [3], although this technique relies on small tip angle rf pulses that may yield insufficient S/N on low-field systems.

2.5. Sensitivity to frequency offsets and rf inhomogeneities

Conceptually, the driven equilibrium preparation in the DECPMG sequence could be replaced by any manipulation of the spin

ensemble that generates a non-vanishing driven equilibrium. In the fast pulsing regime, all such driven equilibria depend on the relaxation times only through their ratio T_1/T_2 and an analogous analysis can be applied to extract this ratio from the ratio of the measured echo amplitudes. However, many potential preparation sequences such as the Steady-State-Free-Precession (SSFP) sequence [32,33] are very sensitive to small offsets in the Larmor frequency. The particular implementation shown in Fig. 1 based on the DEFT sequence with two 180° pulses was selected due to its relative insensitivity to frequency offsets and rf inhomogeneities, although it is essential to refocus the magnetisation during the τ_2 periods with 180° pulses. In addition, as was first pointed out by Waugh [34], it is advantageous to use a DEFT sequence with two 180° pulses rather than a single 180° pulse to improve the compensation for small $\mathbf{B}_1$ inhomogeneities.

To quantify the sensitivity of the sequence in Fig. 1 to offsets in Larmor frequency ω_0 and $\mathbf{B}_1$ inhomogeneities, it is necessary to extend the theoretical analysis to off-resonance and mis-set pulses. In the case of an ideal system, the equilibrium magnetisation obtained as $p \to \infty$ can be determined simply by applying the rotation matrices of the pulses to an initial z magnetisation of M_0 and accounting for relaxation during the time intervals τ_1 and τ_2. If we include the possibility for an offset $\Delta\omega_0$ between the rf spin nutation frequency $\omega_{\rm rf}$ and the Larmor frequency $\gamma|\mathbf{B}_0|$ (where γ is the gyromagnetic ratio and $|\mathbf{B}_0|$ is the magnitude of the static magnetic field) such that

$$\Delta\omega_0 \equiv (\omega_{\rm rf} - \gamma|\mathbf{B}_0|), \tag{15}$$

then the actual nutation frequency of the spins will be given by

$$\Omega = \sqrt{\Delta\omega_0^2 + \omega_1^2}, \tag{16}$$

where $\omega_1 = |\mathbf{B}_1|/2\gamma$ is the amplitude of the rf field in frequency units; on resonance $\Omega = \omega_1$. Assuming the pulse duration t_p is much less than the average relaxation time constants, such that $t_p \ll \langle T_1\rangle$ and $\langle T_2\rangle$, then the general rotation $\mathscr{R}$ can be determined by solving the Bloch equations without relaxation [35]. A 90° pulse along the $\pm x$-axis, acting on an arbitrary magnetisation $\mathbf{m} = M_{x0}\hat{x} + M_{y0}\hat{y} + M_{z0}\hat{z}$, is described by the rotation operators

$$\mathscr{R}_{\pm 90x}\{\hat{x}\} = \begin{pmatrix} \frac{\omega_1^2}{\Omega^2} + \frac{\Delta\omega_0^2}{\Omega^2}\cos\Omega t_{90} \\ \frac{\Delta\omega_0}{\Omega}\sin\Omega t_{90} \\ \pm\frac{\Delta\omega_0\omega_1}{\Omega^2}(1-\cos\Omega t_{90}) \end{pmatrix}, \tag{17}$$

$$\mathscr{R}_{\pm 90x}\{\hat{y}\} = \begin{pmatrix} -\frac{\Delta\omega_0}{\Omega^2}\sin\Omega t_{90} \\ \cos\Omega t_{90} \\ \pm\frac{\omega_1}{\Omega}\sin\Omega t_{90} \end{pmatrix}, \tag{18}$$

and

$$\mathscr{R}_{\pm 90x}\{\hat{z}\} = \begin{pmatrix} \pm\frac{\Delta\omega_0\omega_1}{\Omega^2}(1-\cos\Omega t_{90}) \\ \mp\frac{\omega_1}{\Omega}\sin\Omega t_{90} \\ \frac{\Delta\omega_0^2}{\Omega^2} + \frac{\omega_1^2}{\Omega^2}\cos\Omega t_{90} \end{pmatrix}. \tag{19}$$

In the case of the initial excitation pulse, where it is assumed all the spins are on the z-axis, only Eq. (19) will give a non-zero result. To obtain the rotation matrices for a 180° pulse, t_{90} is replaced by t_{180}, and $\hat{x}$ and $\hat{y}$ are exchanged throughout Eqs. (17)–(19).

The spin relaxation during the arbitrary time interval τ_i will be given by the operator [36]:

$$\mathscr{O}(i)\{\mathbf{m}\} = \left[\Gamma_{i,1}(\mathbf{m}\cdot\hat{z}) + (1-\Gamma_{i,1})\right]\hat{z} + \Gamma_{i,2}[\mathbf{m} - (\mathbf{m}\cdot\hat{z})\hat{z}], \tag{20}$$

normalised to the thermal equilibrium magnetisation M_0. Recalling $\tau_2 = 4\tau_{\rm SE}$, the magnetisation vector of the $(P+1)^{\rm th}$ echo, $\mathbf{m}_{P+1}$, will be given by

$$\mathbf{m}_{P+1} = \left[\mathscr{O}({\rm SE})\mathscr{R}_{180y}\mathscr{O}({\rm SE})\mathscr{R}_{+90x}\mathscr{O}(1)\mathscr{R}_{-90x}\mathscr{O}({\rm SE})\mathscr{R}_{180y}\mathscr{O}({\rm SE})\right]\{\mathbf{m}_P\}. \tag{21}$$

Simulated data that illustrates the sensitivity of the DECPMG sequence to offsets in Larmor frequencies and rf inhomogeneities are shown in Fig. 2.

The results in Fig. 2a demonstrate that the sequence is well compensated for small frequency offsets between the rf and Larmor frequency, provided that the rf pulse power is uniform across the sample and the pulses are set accurately. Since the maximum frequency offset Δf_0 considered here (2 kHz) is much smaller than the nutation frequency $\gamma|\mathbf{B}_1|/2\pi = 34.7$ kHz, the pulses still act as near-perfect 90° and 180° pulses over the whole range.

In the presence of significant rf inhomogeneities, the frequency dependence of the driven equilibrium magnetisation is much more pronounced and is rather complicated, as shown in Fig. 2b. At an rf inhomogeneity of ±20%, the nominal 90° pulses transform the transverse magnetisation into longitudinal magnetisation and back imperfectly. Although the details of the frequency dependence are complicated and are affected by all parameters of the pulse sequence, some of the overall features can be understood with a simple analysis as follows: with inhomogeneous rf fields, longitudinal magnetisation at the end of a given τ_1 interval will, in general, not be restored exactly into the longitudinal direction at the beginning of the next τ_1 interval. Instead, some residual transverse magnetisation will remain in the subsequent τ_1 interval. If the accumulated phase of this transverse component during τ_1 is close to a multiple of 2π, the residual components from different repeating units will add coherently and will lead to a large deviation in the resulting observed equilibrium magnetisation M_{de} from the ideal value.

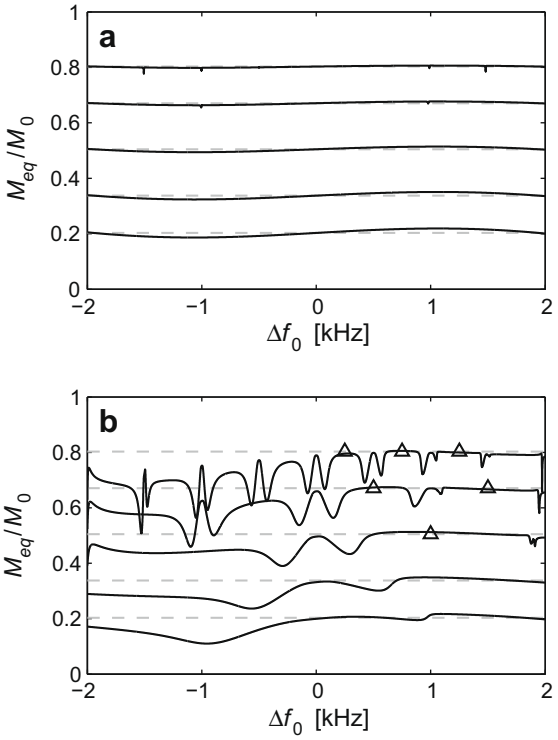

Fig. 2. Simulated variation in M_{de}/M_0 generated by the DECPMG sequence as a function of rf frequency offset Δf_0. The calculations were performed assuming the following parameters: $t_{180} = 2t_{90} = 14.4$ μs, $\tau_2 = 500$ μs and $T_1 = T_2 = 100$ ms. The five curves show results for different values of τ_1: 125 μs (bottom), 250 μs, 500 μs, 1 ms and 2 ms (top). In (a), the rf field is uniform. In (b), we include a uniform distribution of $\mathbf{B}_1$ between 80% and 120% of its nominal value. In both panels, the dashed lines show the ideal on-resonance value, Eq. (2). The triangles in (b) indicate frequency offsets of $\Delta f_0 = (k-1/2)/\tau_1, (k = 1, 2, 3)$ where the effects of rf inhomogeneities are compensated to a higher degree, as discussed in the text.

Using the same argument, when the precession of the transverse component during τ_1 is close to an odd multiple of π, subsequent contributions tend to cancel and the observed value of M_{de} is affected less by rf inhomogeneities. This occurs at offset frequencies $\Delta f_{0,k} = (k - 1/2)/\tau_1$, where k is an integer. It is apparent that at these offset frequencies, indicated in Fig. 2b as triangles for $k = 1, 2, 3$, the deviations of M_{de} from the ideal values are indeed much reduced. It is therefore preferable to perform the DECPMG measurements at such offset frequencies.

There is interest in applying the DECPMG approach to stray field [37] or portable [38] NMR applications. The simulation results above indicate that in the presence of inhomogeneities of the static and rf field, the response of the standard DECPMG sequence can become very complicated. In future work we will consider ways in which the basic DECPMG pulse sequence presented here can be modified or optimised to suit these devices.

3. Surface relaxation

It is well known that nuclear spins moving on a pore surface will undergo enhanced relaxation due to interactions with relaxation sinks, such as paramagnetic ions, in the porous solid. If the pore has a large surface-to-volume ratio S/V, then the liquid molecules on the pore surface will exchange with those in the bulk on a time short compared to the experimental observation time [39]. Therefore, the observed, frequency dependent longitudinal relaxation rate will be

$$\frac{1}{T_{1,\mathrm{obs}}(\omega_0)} = \frac{1}{T_{1,\mathrm{bulk}}} + \frac{\epsilon S}{V}\frac{1}{T_{1,\mathrm{surface}}(\omega_0)}, \tag{22}$$

where ϵ is the thickness of the surface layer, assumed to be equal to the diameter of one liquid molecule. In the absence of magnetic field gradients, Eq. (22) can be applied to the transverse relaxation rate by exchanging T_1 and T_2 throughout and accounting for diffusion. Since the surface relaxation rate $1/T_{1,\mathrm{surface}}$ will be the dominant component in Eq. (22) (assuming S/V is large), it would be necessary to determine the surface relaxation rate in order to extract a value for S/V. Korb et al. proposed a theory to describe surface relaxation rates [40,41]. If liquid molecules (proton spin I) are in close proximity to a surface containing paramagnetic impurities (electron spin S), some of the liquid molecules will undergo a two-dimensional random walk across the pore surface at a rate defined by τ_m (the surface diffusion correlation time), for a time τ_s (the surface residency time). From this model, values of $T_{1,\mathrm{surface}}$ and $T_{2,\mathrm{surface}}$ can be calculated theoretically, although determining accurate values from experimental results has been shown elsewhere to be complicated [11]. However, the ratio of relaxation rates $T_{2,\mathrm{surface}}/T_{1,\mathrm{surface}}$ resolves to a function of ω_I, τ_m, and τ_m/τ_s only:

$$\frac{T_{2,\mathrm{surface}}(\omega_0)}{T_{1,\mathrm{surface}}(\omega_0)} = 2\left\{\frac{3\ln\left(\frac{1+\omega_I^2\tau_m^2}{\left(\frac{\tau_m}{\tau_s}\right)^2+\omega_I^2\tau_m^2}\right) + 7\ln\left(\frac{1+\omega_S^2\tau_m^2}{\left(\frac{\tau_m}{\tau_s}\right)^2+\omega_S^2\tau_m^2}\right)}{4\ln\left(\left(\frac{\tau_m}{\tau_s}\right)^{-2}\right) + 3\ln\left(\frac{1+\omega_I^2\tau_m^2}{\left(\frac{\tau_m}{\tau_s}\right)^2+\omega_I^2\tau_m^2}\right) + 13\ln\left(\frac{1+\omega_S^2\tau_m^2}{\left(\frac{\tau_m}{\tau_s}\right)^2+\omega_S^2\tau_m^2}\right)}\right\}. \tag{23}$$

Therefore, from Eq. (22) (assuming S/V is large, $T_{1,\mathrm{surface}} \ll T_{1,\mathrm{bulk}}$, and $T_{2,\mathrm{surface}} \ll T_{2,\mathrm{bulk}}$, as is often the case in low-field measurements of porous materials) the ratio $T_{1,\mathrm{obs}}/T_{2,\mathrm{obs}}$, determined as a function of magnetic field strength $|\mathbf{B}_0|$, can be used to estimate directly the surface diffusion correlation and residency times. At higher magnetic field strengths, $T_{1,\mathrm{surface}} \to T_{1,\mathrm{bulk}}$ (and likewise for T_2) so it will be necessary to subtract the relaxation times for bulk liquid from the observed times to calculate the ratio $T_{2,\mathrm{surface}}/T_{1,\mathrm{surface}}$.

4. Experimental

4.1. Materials and methods

The DECPMG measurements were conducted on magnets with four different field strengths of 0.05, 0.3, 2, and 9.4 T, corresponding to ^{1}H (proton) resonant frequencies of $f_0 = 2$, 12, 85, and 400 MHz, respectively. The low-field permanent magnets ($f_0 = 2$ and 12 MHz) were manufactured by Oxford Instruments and controlled via a Maran DRX spectrometer console. The optimum 90° and 180° pulse durations were $t_{90} = 7.2$ μs and $t_{180} = 14.4$ μs (2 MHz), and $t_{90} = 8.3$ μs and $t_{180} = 17.5$ μs (12 MHz). The CPMG echo spacing was $2\tau_{\mathrm{CPMG}} = 1$ ms for both magnets. The values of τ_1 and τ_2 were selected for each magnet as explained in Section 4.2. The high-field superconducting magnets ($f_0 = 85$ and 400 MHz) were controlled via Bruker AV spectrometer consoles. The optimum 90° pulses were of duration $t_{90} = 15$ μs (85 MHz) and $t_{90} = 65$ μs ($f_0 = 400$ MHz). For both magnets, $t_{180} = 2t_{90}$. The CPMG echo spacing was $2\tau_{\mathrm{CPMG}} = 2$ ms. Again, τ_1 and τ_2 were selected as explained in Section 4.2.

The $T_1 - T_2$ correlation experiment consists of an inversion (180°) pulse followed by a variable recovery delay T_{RD}, and then a CPMG echo train. Further details of this pulse sequence can be found in reference [2]. The T_1 recovery delay was varied logarithmically over the range $T_{RD} = 10$ ms to 10 s in 32 steps. The CPMG echo spacing was $2\tau_{\mathrm{CPMG}} = 1$ ms for the low-field magnets and $2\tau_{\mathrm{CPMG}} = 2$ ms for the high-field magnets. 1024 echoes were obtained typically, although only the even echo intensities were used in the analysis. The data was inverted using the Fast Laplace Inversion (FLI) algorithm [1].

A bulk water sample, doped with gadolinium (Gd^{3+}) to increase the longitudinal and transverse relaxation rates equally, was used to optimise the DECPMG pulse sequence. At $f_0 = 12$ MHz the doped water exhibited $T_1 = T_2 = 0.08$ s.

The rock samples studied were Bentheimer sandstone and Portland limestone. These are both high permeability rocks with porosities of $\varphi = 0.24$ and 0.18, respectively. The rock samples comprised of cylindrical cores having external dimensions of 60 × 38 mm (length × diameter). The cores were vacuum saturated with either 2 wt. % KCl brine solution (water) to prevent osmotic swelling of the clay content in the sandstone, or dodecane (oil). The cores were placed in air-tight polytetrafluoroethene (PTFE) cups for the duration of the NMR measurements. The DECPMG measurements on the rock cores had a duration of 10 min (with a repeat delay of 10 s and 16 scans). The $T_1 - T_2$ measurements (with 32 T_{RD} times, 10 s repeat delays, and 16 scans) had an approximate duration of 2 h.

4.2. Optimisation

As is shown in Fig. 3, the highest sensitivity is achieved by choosing the intervals τ_1 and τ_2 such that τ_1/τ_2 is close to the expected ratio of T_1/T_2, whilst keeping them short enough so that the fast pulsing regime still applies. For this case, $A_D = A_C/2$. Unless a large difference between T_1 and T_2 is expected, a value of $0.5 \leqslant \tau_2/\tau_1 \leqslant 1$ should be a suitable starting point. It is important to use an accurate value for the ratio of τ_1/τ_2, and care should be taken to include any timing errors, such as finite pulse durations, in the calculation as necessary.

Since the equilibrium magnetisation at the end of the DE encoding portion of the pulse sequence is independent of the starting magnetisation, the DECPMG scan can be acquired immediately after the CPMG reference scan to offer a further reduction in experimental time. However, this can generate high rf duty

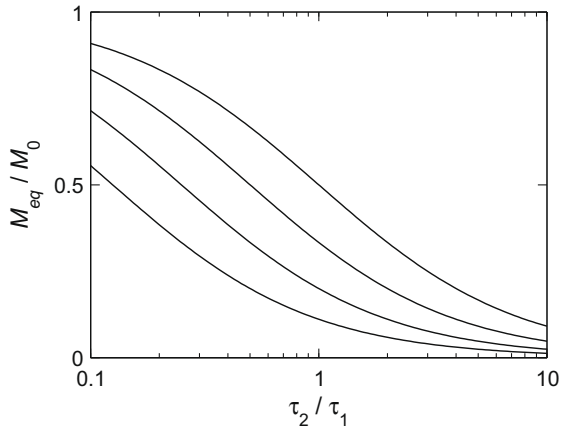

Fig. 3. Simulated variation in M_{de}/M_0 as a function of the ratio of the DECPMG pulse sequence time intervals τ_2/τ_1. The lines (top to bottom) show the ideal magnetisation for $\langle T_1/T_2\rangle = 1, 2, 4$, and 8. The highest sensitivity of M_{de}/M_0 with respect to T_1/T_2 is observed when $\tau_2/\tau_1 = \langle T_1/T_2\rangle^{-1}$.

cycles if τ_1 and τ_2 are short and care must be taken not to heat the sample or damage the spectrometer electronics.

The B_0 field of permanent magnet systems can vary during the course of an experiment (due primarily to thermal variations in the magnet poles), resulting in a variation of the associated Larmor frequency. This corresponds to a variation in $\gamma|\mathbf{B}_0|$ and hence, from Eq. (15), a variation in $\Delta\omega_0$. The simulations presented in Fig. 2 indicate that with accurately set pulse widths, small mis-matches in the rf frequency are not important as long as the rf field is uniform across the sample.

Fig. 4a shows the variation of M_{de}/M_0 as a function of an imposed frequency offset Δf_0 for the doped water sample at $f_0 = 12$ MHz. It can been seen that the maximum values of M_{de}/M_0 for each value of τ_1 correspond well to those for the ideal response given by Eq. (2). For long τ_1 intervals, M_{de}/M_0 is reduced due to diffusive attenuation of the residual magnetisation in the $x-y$ plane. These oscillations are more pronounced for the doped water sample at $f_0 = 2$ MHz, Fig. 4b. A comparison of the experimental results in Fig. 4b with the simulations in Fig. 2b shows remarkable qualitative similarities. Finite $\mathbf{B}_0$ homogeneity in the experiments averages out some of the rapid oscillations found in the simulations. Together, Figs. 2 and 4 indicate that the main cause in the difference in response at $f_0 = 12$ and 2 MHz is rf inhomogeneity; this has been confirmed by experimental estimates of $\Delta\mathbf{B}_1$. At $f_0 = 12$ MHz, $|\Delta\mathbf{B}_1|/|\mathbf{B}_1| \approx 0.1$; at $f_0 = 2$ MHz, $|\Delta\mathbf{B}_1|/|\mathbf{B}_1| \approx 0.25$.

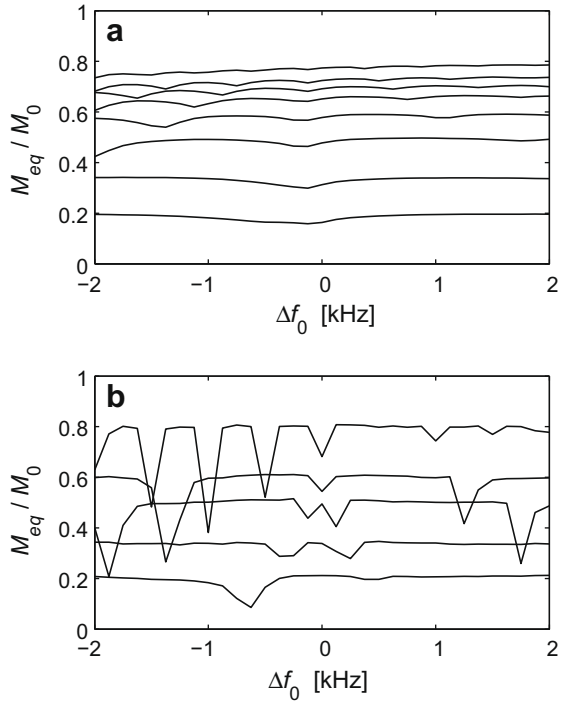

Fig. 4. Observed variation in M_{de}/M_0 as a function of an imposed frequency offset $\Delta\omega_0$ for a doped water sample at (a) $f_0 = 12$ and (b) 2 MHz. In all cases $\tau_2 = 500$ μs. In (a), the lines represent τ_1 times of 125 μs (bottom), 250 μs, 500 μs, 800 μs, 1 ms, 1.2 ms, 1.5 ms, and 2 ms (top). In (b), the lines represent τ_1 times of 125 μs (bottom), 250 μs, 500 μs, 1 ms, and 2 ms (top).

For both magnets, with $\tau_1 = \tau_2 = 500$ μs, the correct observed equilibrium magnetisation is obtained at an offset frequency of $\Delta f_0 = \pm 1$ kHz. The precise location of the oscillations has been seen to depend on the quality of the rf pulse durations: imperfect or mismatched pulses will add an additional frequency offset. Since only the depth of the oscillations depends on the magnitude of the magnetic field inhomogeneities, the same optimised frequency offset can be used for all samples. Magnetic susceptibility induced field gradients in the rock samples will not affect the position of the oscillations.

5. Results and discussions

5.1. Validation

To validate the results from the DECPMG pulse sequence, the $\langle T_1/T_2\rangle_{T_2}$ ratio of a doped water sample was measured at $f_0 = 12$ MHz. The increased longitudinal relaxation rate allowed a shorter repetition delay to be used between successive scans but was otherwise inconsequential to the application of the pulse sequence. Fig. 5a shows the distribution of T_2 relaxation times obtained from the DECPMG sequence, $A_D(\log T_2)$ (solid line), and from the CPMG reference scan, $A_C(\log T_2)$ (dashed line). Using Eq. (14), the average $\langle T_1/T_2\rangle$ ratio has been determined as a function of T_2, see Fig. 5b. In this case $\langle T_1/T_2\rangle_{T_2} = 1.0 \pm 0.1$ as expected. The ratio $A_D/A_C = M_{de}/M_0$ is seen to be approximately constant across the range of T_2 relaxation times as indicated by the grey scale. This is in agreement with the full two-dimensional $T_1 - T_2$ plot of $g_2(\log T_2, \log T_1)$ shown in Fig. 5c for the same sample where the single relaxation time component is centred on the diagonal line $T_1 = T_2$.

5.2. Permeable rocks

In Fig. 6a, T_1/T_2 as a function of T_2 is shown for a typical Bentheimer sandstone saturated with brine solution, at $f_0 = 12$ MHz. Averaged across the entire sample, $\langle T_1/T_2\rangle_{T_2} = 1.8 \pm 0.2$, where the majority of the signal is contained in a dominant component centred on $T_2 = 1$ s (as indicated by the colour scale). The results can be displayed as average T_1 versus T_2, defined by $\langle T_1\rangle_{T_2} \equiv T_2 \cdot \langle T_1/T_2\rangle_{T_2}$. In Fig. 6b the $\langle T_1\rangle_{T_2}$ data from (a) has been overlaid on a plot of the $T_1 - T_2$ distribution function, $g_2(\log T_2, \log T_1)$, obtained from the same sample. Good agreement is seen between the two data sets. The $T_1 - T_2$ correlation plot shows a single dominant peak lying diagonal to the line $T_1 = T_2$ (lower diagonal line), with a tail extending to shorter relaxation times. The peak is centred on $T_1 = 1.56$ s and $T_2 = 0.98$ s, suggesting $T_1/T_2 = 1.6$ for this rock. However, the DECPMG data gives $\langle T_1/T_2\rangle_{T_2} = 1.8$ (upper diagonal line) because it is determined from a weighted average across the entire sample. A more detailed statistical analysis of the entire $T_1 - T_2$ correlation data provides the

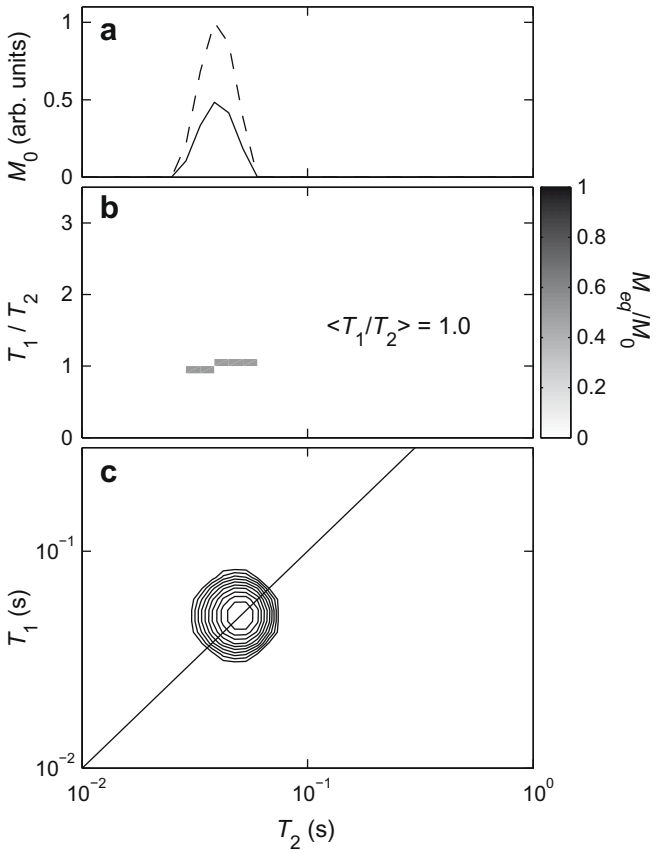

Fig. 5. Measurements of a doped water sample at $f_0 = 12$ MHz: (a) The T_2 distributions from the DECPMG data (solid line) and the CPMG reference data (dashed line); (b) T_1/T_2 as a function of T_2 from the DECPMG experiment. The grey scale indicates the signal intensity M_{de}/M_0; (c) a two-dimensional $T_1 - T_2$ correlation plot confirming $T_1 = T_2$ in this sample (diagonal line).

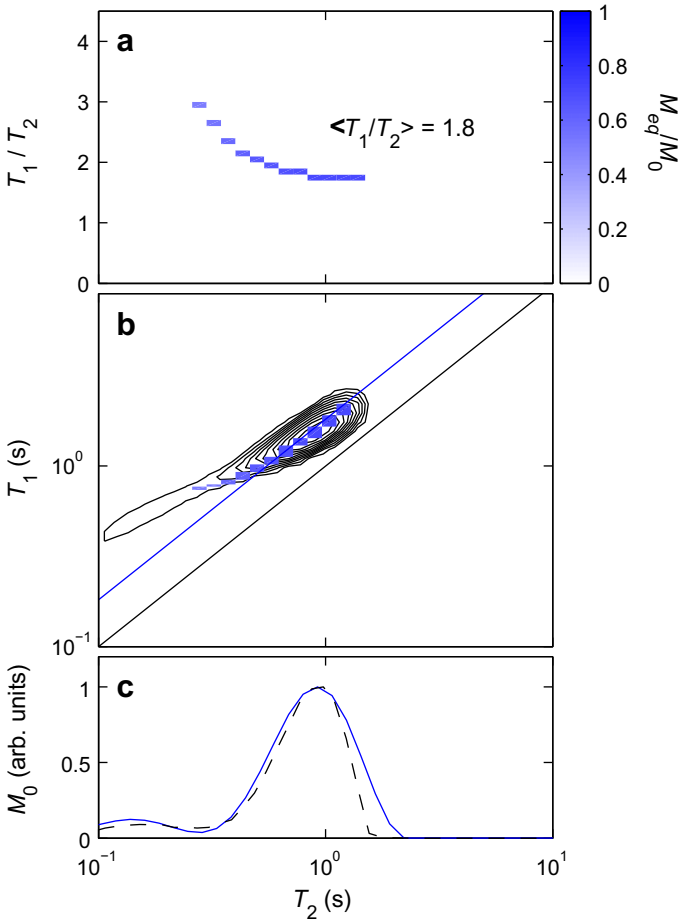

Fig. 6. (a) T_1/T_2 as a function of T_2 for a water saturated sandstone rock core determined from DECPMG data at $f_0 = 12$ MHz. The colour scale indicates the intensity of M_{de}/M_0. (b) The two-dimensional $T_1 - T_2$ correlation plot for the same sample. The DECPMG data has been overlaid for comparison. The lower (black) diagonal line indicates where $T_1 = T_2$; the upper (blue) diagonal line indicates where $T_1 = 1.8T_2$. (c) The T_2 distributions determined from the DECPMG data (solid blue line) and the projection onto the T_2 axis from the $T_1 - T_2$ correlation (dashed black line).

same value of $\langle T_1/T_2 \rangle$ as determined from the DECPMG experiment. It can also be seen in Fig. 6c that the one-dimensional T_2 distributions determined via the DECPMG and the $T_1 - T_2$ correlation experiments are equivalent.

Identifying multi-component liquid fractions, specifically oil and water in rocks, is an important aspect in reservoir engineering. On low-field NMR systems this is achieved conventionally by studying distributions of T_1 or T_2 data, or $D - T_2$ correlations [4,10]. In time sensitive measurements it may be necessary to rely on T_2 distributions alone. In Fig. 7a, one-dimensional T_2 distributions for sandstones containing either water (blue) or oil (green) are shown, determined at $f_0 = 2$ MHz. These distributions reveal a distinct difference but subtle difference: the water exhibits a higher modal T_2 than the oil. The DECPMG data for the same samples are shown in Fig. 7b. The addition of the $\langle T_1 \rangle_{T_2}$ relaxation time provides a more distinct segregation of the water (blue) and oil (green) signals. For the water, $\langle T_1/T_2 \rangle_{T_2} = 1.5 \pm 0.2$; for the oil, $\langle T_1/T_2 \rangle_{T_2} = 1.1 \pm 0.1$. This systematic difference in the ratio of transverse to longitudinal relaxation time reflects differences in the detailed relaxation mechanism for oil and water molecules [42]. The measurement of $\langle T_1/T_2 \rangle_{T_2}$ might therefore be useful in quantifying the fractions of oil and water present in reservoir rocks.

In the measurement of CPMG decays from oils, there is a potential problem associated with homonuclear coupling [25]. However, the experiments presented here all occur in the fast pulsing regime and so the criteria $2J\tau_{CPMG} \ll 1$ (where J is the coupling constant) is satisfied.

5.3. Surface interactions

Wettability is another topic of current interest in reservoir engineering. Although some promising methods have been proposed recently to relate NMR relaxation parameters and wettability [43–46], mixed wettability surfaces are still difficult to characterise [47]. The T_1/T_2 ratio can be used to estimate the average surface residency time of liquid molecules in a pore. These measurements provide a relative strength of surface interaction, hence indicating whether a pore is preferentially oil or water wet. As an example, the average $\langle T_1/T_2 \rangle_{T_2}$ ratio was determined using DECPMG for water in sandstone and limestone rock cores over a range of ^{1}H resonance frequencies ω_0. At the highest frequency (corresponding to the highest magnetic field strength) the T_2 measurement is influenced strongly by diffusion in internal magnetic field gradients induced by the susceptibility difference at the rock/water interface [48–50]. These internal gradients have been shown to scale with magnetic field strength [51]. We will consider the influence of magnetic field strength on T_2 measurements in more detail in a future publication. A similar situation could arise for measurements in the inhomogeneous fields of unilateral magnets, where the CPMG portion may require additional optimisation [36]. Here,

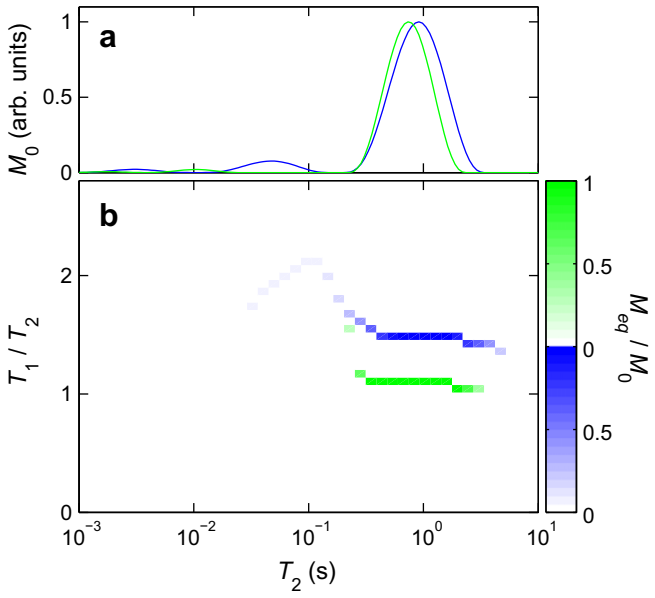

Fig. 7. (a) One-dimensional T_2 distributions obtained from CPMG data of water (blue) and oil (green) in sandstone rock cores at $f_0 = 2$ MHz. (b) DECPMG data showing T_1/T_2 as a function of T_2 for the same liquids. The colour scale indicates the intensity of M_{de}/M_0 for each liquid.

the fit to the $\langle T_1/T_2\rangle_{T_2}$ data is weighted heavily in favour of the measurements at the lower frequencies where in the influence of the internal gradients is less significant. The results are shown in Fig. 8, including lines of best fit to Eq. (23). For the sandstone, $\tau_m = 6\times10^{-10}$ s and $\tau_s = 1\times10^{-6}$ s. For the limestone, $\tau_m = 5\times10^{-10}$ s and $\tau_s = 1\times10^{-7}$ s. Both the surface diffusion correlation and residency times are shorter in the limestone than in the sandstone, suggesting the water has a stronger interaction with the sandstone surface.

6. Conclusion

In this paper we presented the Driven-Equilibrium Carr–Purcell Meiboom–Gill (DECPMG) pulse sequence as a rapid method of determining the $\langle T_1/T_2\rangle$ ratio as a function of T_2 and demonstrated the applicability of the measurement to the study of oil reservoir rocks. The DECPMG pulse sequence has been shown to provide the same mean value of $\langle T_1/T_2\rangle$ as determined from two-dimensional $T_1 - T_2$ relaxation correlations plots for a doped water sample and for brine solution in a permeable sandstone. The rapid data acquisition makes the DECPMG sequence suitable for use in time sensitive measurements. The DECPMG experiment has also been proposed as a potential rapid method for identifying oil and water in rocks, and for estimating surface residency times when $\langle T_1/T_2\rangle_{T_2}$ is measured as a function of the resonant frequency. Additionally, the pulse sequence could be used to reduce the experimental time required to determine flow propagators without relaxation time weighting, as presented elsewhere [13]: a method that requires $\langle T_1/T_2\rangle$ to be determined as a function of T_2.

The DECPMG pulse sequence does require some initial calibration since the correct driven equilibrium magnetisation M_{de} will depend on the frequency offset from resonance $\Delta\omega_0$ in inhomogeneous magnetic fields. Nevertheless, this pulse sequence can be implemented on a wide range of magnet systems, including unilateral (portable) devices, and offers unambiguous data that is straightforward to analyse and interpret accurately.

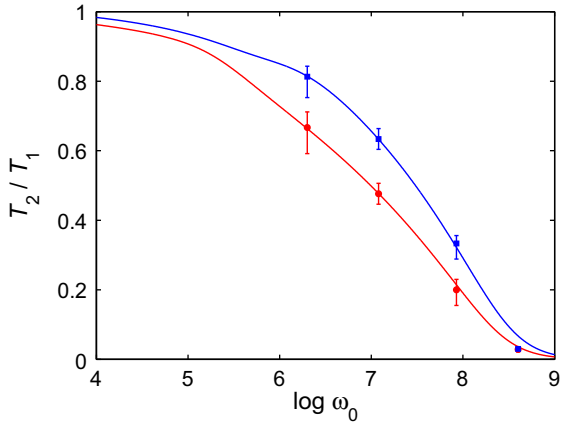

Fig. 8. The inverse T_1/T_2 ratio as a function of proton resonance frequency ω_0 for water in sandstone (•) and limestone (■) rock cores, as determined using the DECPMG sequence implemented at four different magnetic field strengths. Lines of best fit to the data are shown, as explained in the text.

Acknowledgments

For helpful discussions we thank Mr. Thusara Chandrasekera and Dr. Andy Sederman, and we thank Prof. Lynn Gladden for providing access to the high-field magnets. We thank Mr. Olivier Terneaud for the original report on the DECPMG sequence, and Mr. John Staniland for preparing the rock core samples. The author J.M. thanks Schlumberger Cambridge Research for financial support.

References

[1] L. Venkataramanan, Y.Q. Song, M.D. Hürlimann, Solving Fredholm integrals of the first kind with tensor product structure in 2 and 2.5 dimensions, IEEE Trans. Sig. Process. 50 (2002) 1017–1026.
[2] Y.Q. Song, L. Venkataramanan, M.D. Hürlimann, M. Flaum, P. Frulla, C. Straley, $T_1 - T_2$ correlation spectra obtained using a fast two-dimensional Laplace inversion, J. Magn. Reson. 154 (2002) 261–268.
[3] T.C. Chandrasekera, J. Mitchell, E.J. Fordham, L.F. Gladden, M.L. Johns, Rapid encoding of T_1 with spectral resolution in n-dimensional relaxation correlations, J. Magn. Reson. 194 (2008) 156–161.
[4] M.D. Hürlimann, L. Venkataramanan, Quantitative measurement of two-dimensional distribution functions of diffusion and relaxation in grossly inhomogeneous fields, J. Magn. Reson. 157 (2002) 31–42.
[5] P.J. McDonald, J.P. Korb, J. Mitchell, L. Monteilhet, Surface relaxation and chemical exchange in hydrating cement pastes: a two-dimensional NMR relaxation study, Phys. Rev. E 72 (2005) 011409.
[6] K.E. Washburn, P.T. Callaghan, Tracking pore to pore exchange using relaxation exchange spectroscopy, Phys. Rev. Lett. 97 (2006) 175502.
[7] P.T. Callaghan, I. Furo, Diffusion–diffusion correlation and exchange as a signature for local order and dynamics, J. Chem. Phys. 120 (2004) 4032–4038.
[8] B.Q. Sun, K.J. Dunn, Two-dimensional nuclear magnetic resonance petrophysics, Magn. Reson. Imaging 23 (2005) 259–262.
[9] R.J.S. Brown, R. Chandler, J.A. Jackson, R.L. Kleinberg, M.N. Miller, Z. Paltiel, M.G. Prammer, History of NMR well logging, Concept. Magn. Reson. 13 (2001) 335–413.
[10] M.D. Hürlimann, M. Flaum, L. Venkataramanan, C. Flaum, R. Freedman, G.J. Hirasaki, Diffusion-relaxation distribution functions of sedimentary rocks in different saturation states, Magn. Reson. Imaging 21 (2003) 305–310.
[11] L. Monteilhet, J.P. Korb, J. Mitchell, P.J. McDonald, Observation of exchange of micropore water in cement pastes by two-dimensional $T_2 - T_2$ nuclear magnetic resonance relaxometry, Phys. Rev. E 74 (2006) 061404.
[12] D. Weber, J. Mitchell, J. McGregor, L.F. Gladden, Determining relative strengths of interaction for reactants and solvents in catalysts, J. Phys. Chem. C 113 (2009) 6610–6615.
[13] J. Mitchell, D.A. Graf von der Schulenburg, D.J. Holland, E.J. Fordham, M.L. Johns, L.F. Gladden, Determining NMR flow propagator moments in porous rocks without the influence of relaxation, J. Magn. Reson. 193 (2008) 218–225.
[14] M.D. Hürlimann, O.J. Terneaud, D. Freed, U. Scheven, L. Venkataramanan, Nuclear magnetic resonance methods for extracting information about a fluid in a rock, US patent EP1301810 B1, 2008.
[15] H. Carr, E. Purcell, Effects of diffusion on free precession in NMR experiments, Phys. Rev. 94 (1954) 630–638.

[16] S. Meiboom, D. Gill, Modified spin-echo method for measuring nuclear relaxation times, Rev. Sci. Instrum. 29 (1958) 668–691.
[17] A. Schwenk, Steady-state techniques for low sensitivity and slowly relaxing nuclei, Prog. Nucl. Magn. Reson. Spectrosc. 17 (1985) 69–140.
[18] A.D. Bain, W.P.Y. Ho, J.S. Martin, A new way of measuring NMR spin–spin relaxation times (T_2), J. Magn. Reson. 43 (1981) 328–330.
[19] J. Kronenbitter, A. Schwenk, A new technique for measuring the relaxation times T_1 and T_2 and the equilibrium magnetization M_0 of slowly relaxing systems with weak NMR signals, J. Magn. Reson. 25 (1977) 147–165.
[20] L.C. Headley, W.E. Wallace, P. Waldstein, Reversed Carr–Purcell train for measurement of NMR relaxation times by approach to driven equilibrium, J. Appl. Phys. 44 (1973) 5624–5625.
[21] E.D. Becker, J.A. Ferretti, T.C. Farrar, Driven equilibrium Fourier transform spectroscopy: a new method for nuclear magnetic resonance signal enhancement, J. Am. Chem. Soc. 91 (1969) 7784–7785.
[22] E.L. Hahn, Spin echoes, Phys. Rev. 80 (1950) 580–594.
[23] R.R. Shoup, E.D. Becker, T.C. Farrar, The driven equilibrium fourier transform NMR technique: an experimental study, J. Magn. Reson. 8 (1972) 298–310.
[24] C.J. Turner, Multipulse NMR in liquids, Prog. Nucl. Magn. Reson. Spectrosc. 16 (1984) 311–370.
[25] A. Allerhand, Analysis of Carr–Purcell spin-echo NMR experiments on multiple-spin systems. I. The effect of homonuclear coupling, J. Chem. Phys. 44 (1966) 1–9.
[26] H.T. Edzes, An analysis of the use of pulse multiplets in the single scan determination of spin-lattice relaxation rates, J. Magn. Reson. 17 (1975) 301–313.
[27] R. Vold, J. Waugh, M. Klein, D. Phelps, Measurement of spin relaxation in complex systems, J. Chem. Phys. 48 (1968) 3831–3832.
[28] E.J. Fordham, A. Sezginer, L.D. Hall, Imaging multiexponential relaxation in the (y, $\log_e T_1$) plane, with applications to clay filtration in rock cores, J. Magn. Reson. A 113 (1995) 139–150.
[29] J.P. Butler, J.A. Reeds, S.V. Dawson, Estimating solutions of 1st kind integral-equations with nonnegative constraints and optimal smoothing, SIAM J. Numer. Anal. 18 (3) (1981) 381–397.
[30] G. Wahba, Practical approximate solutions to linear operator equations when data are noisy, SIAM J. Numer. Anal. 14 (1977) 651–667.
[31] J.D. Wilson, Statistical approach to the solution of 1st-kind integral-equations arising in the study of materials and their properties, J. Mater. Sci. 27 (1992) 3911–3924.
[32] R. Bradford, C. Clay, E. Strick, A steady-state transient technique in nuclear induction, Phys. Rev. 84 (1951) 157–158.
[33] H.Y. Carr, Steady-state free precession in nuclear magnetic resonance, Phys. Rev. 112 (1958) 157–158.
[34] J.S. Waugh, Sensitivity in Fourier transform NMR spectroscopy of slowly relaxing systems, J. Mol. Spectrosc. 35 (1970) 298–305.
[35] F. Bloch, Nuclear induction, Phys. Rev. 70 (1946) 460–474.
[36] M.D. Hürlimann, D.D. Griffin, Spin dynamics of Carr–Purcell–Meiboom–Gill-like sequences in grossly inhomogeneous B_0 and B_1 fields and application to NMR well logging, J. Magn. Reson. 143 (2000) 120–135.
[37] P.J. McDonald, Stray field magnetic resonance imaging, Prog. Nucl. Magn. Reson. Spectrosc. 30 (1997) 69–99.
[38] J. Mitchell, P. Blumler, P.J. McDonald, Spatially resolved nuclear magnetic resonance studies of planar samples, Prog. Nucl. Magn. Reson. Spectrosc. 48 (2006) 161–181.
[39] K.R. Brownstein, C.E. Tarr, Importance of classical diffusion in NMR studies of water in biological cells, Phys. Rev. A 19 (1979) 2446–2453.
[40] J.P. Korb, M. Whaley-Hodges, R.G. Bryant, Translational diffusion of liquids at surfaces of microporous materials: theoretical analysis of field-cycling magnetic relaxation measurements, Phys. Rev. E 56 (1997) 1934–1945.
[41] J.P. Korb, M. Whaley-Hodges, T. Gobron, R.G. Bryant, Anomalous surface diffusion of water compared to aprotic liquids in nanopores, Phys. Rev. E 60 (1999) 3097–3106.
[42] J.P. Korb, S. Godefroy, M. Fleury, Surface nuclear magnetic relaxation and dynamics of water and oil in granular packings and rocks, Magn. Reson. Imaging 21 (2003) 193–199.
[43] S.H. Al-Mahrooqi, C.A. Grattoni, A.K. Moss, X.D. Jing, An investigation of the effect of wettability on NMR characteristics of sandstone rock and fluid systems, J. Petrol. Sci. Eng. 39 (2003) 389–398.
[44] R. Freedman, N. Heaton, M. Flaum, G.J. Hirasaki, C. Flaum, M. Hürlimann, Wettability, saturation, and viscosity from NMR measurements, SPE J. 8 (2003) 317–327.
[45] H. Guan, D. Brougham, K.S. Sorbie, K.J. Packer, Wettability effects in a sandstone reservoir and outcrop cores from NMR relaxation time distributions, J. Petrol. Sci. Eng. 34 (2002) 33–52.
[46] W. Looyestijn, J. Hofman, Wettability-index determination by nuclear magnetic resonance, SPE Reservoir Eval. Eng. 9 (2) (2006) 146–153.
[47] E. Toumelin, C. Torres-Verdin, B.Q. Sun, K.J. Dunn, Limits of 2D NMR interpretation techniques to quantify pore size, wettability, and fluid type: a numerical sensitivity study, SPE J. 11 (2006) 354–363.
[48] M.D. Hürlimann, K.G. Helmer, T.M. de Swiet, P.N. Sen, C.H. Sotak, Spin echoes in a constant gradient and in the presence of simple restriction, J. Magn. Reson. A 113 (1995) 260–264.
[49] M.D. Hürlimann, Effective gradients in porous media due to susceptibility differences, J. Magn. Reson. 131 (1998) 232–240.
[50] V. Anand, G.J. Hirasaki, Paramagnetic relaxation in sandstones: distinguishing T_1 and T_2 dependence on surface relaxation, internal gradients and dependence on echo spacing, J. Magn. Reson. 190 (2008) 68–85.
[51] K.E. Washburn, C.D. Eccles, P.T. Callaghan, The dependence on magnetic field strength of correlated internal gradient relaxation time distributions in heterogeneous materials, J. Magn. Reson. 194 (2008) 33–40.